Available online at www.sciencedirect.com
SCIENCE DIRECT®
Carbohydrate Research 340 (2005) 1025–1037
Carbohydrate RESEARCH

Conformational features of cepacian: the exopolysaccharide produced by clinical strains of *Burkholderia cepacia*

Carlos E. Sampaio Nogueira,[a] Jose R. Ruggiero,[a] Paola Sist,[b] Paola Cescutti,[b] Ranieri Urbani[b,*] and Roberto Rizzo[b]

[a]*UNESP Sao Paulo State University, Department of Physics, IBILCE, Sao Jose do Rio Preto, Brazil*
[b]*Department of Biochemistry, Biophysics and Macromolecular Chemistry, University of Trieste, Via Licio Giorgieri 1, 34127 Trieste, Italy*

Received 4 October 2004; accepted 23 December 2004

Dedicated to Professor David A. Brant

Abstract—Conformational energy calculations and molecular dynamics investigations, both in water and in dimethyl sulfoxide, were carried out on the exopolysaccharide cepacian produced by the majority of the clinical strains of *Burkholderia cepacia*, an opportunistic pathogen causing serious lung infection in patients affected by cystic fibrosis, The investigation was aimed at defining the structural and conformational features, which might be relevant for clarification of the structure–function relationships of the polymer. The molecular dynamics calculations were carried out by Ramachandran-type energy plots of the disaccharides that constitute the polymer repeating unit. The dynamics of an oligomer composed of three repeating units were investigated in water and in Me_2SO, a non-aggregating solvent. Analysis of the time persistence of hydrogen bonds showed the presence of a large number of favourable interactions in water, which were less evident in Me_2SO. The calculations on the cepacian chain indicated that polymer conformational features in water were affected by the lateral chains, but were also largely dictated by the presence of solvent. Moreover, the large number of intra-chain hydrogen bonds in water disappeared in Me_2SO solution, increasing the average dimension of the polymer chains.

Keywords: *Burkholderia cepacia*; Exopolysaccharide; Cepacian; Molecular modelling; Molecular dynamics; Polymer chain statistics

1. Introduction

Burkholderia cepacia, originally recognised as an environmental bacterium causing soft rot in onions,[1] is an opportunistic pathogen causing serious lung infections in patients affected by cystic/fibrosis (CF).[2] This is a genetic disease, which causes a modification of the protein involved in the transportation of chloride ions across cellular membranes (the so-called Cystic Fibrosis Transmembrane Regulator, CFTR). Among the consequences, the altered composition of the fluid on the lung epithelium and impairment of the muciliary clearance favour the colonisation by different bacteria. Bacterial infections are the major cause of death for CF patients, whose life expectancy does not exceed 40 years. In fact, *B. cepacia* infection can cause the so-called '*B. cepacia* syndrome', a necrotising pneumonia and septicemia associated with a fatal and rapid decline of the lung functions. Microbiological studies established that *B. cepacia* is a family of bacteria (called '*B. cepacia* complex'), composed of different genomovars, often with identical phenotypes.[3] Up to now, 10 different genomovars have been recognised. Among these, genomovars II, III, and to a lesser extent, genomovar I, are of clinical relevance.[4] Studies carried out on *Pseudomonas*

Abbreviations: MD, molecular dynamics; HB, hydrogen bond; MC, Monte Carlo; Me_2SO, dimethyl sulfoxide.

* Corresponding author. E-mail: urbani@bbcm.units.it

0008-6215/$ - see front matter © 2005 Elsevier Ltd. All rights reserved.
doi:10.1016/j.carres.2004.12.028

aeruginosa, the most threatening opportunistic pathogen involved in CF lung infection, indicate that the exopolysaccharide (alginate) produced 'in vivo' by the bacteria is an important factor in the infection maintenance.[5] Very recently a similar observation was also made in a murine model of CF infected by *B. cepacia*.[6] The exopolysaccharides constitute not only physical barrier around the bacterial colonies that impedes the antimicrobial action of agents either of endogenous or of exogenous origin, but might also specifically interact with components of the host immune system, inhibiting their activation.[7,8]

Structural studies carried out in different laboratories on exopolysaccharides produced by clinical strains of *B. cepacia* have demonstrated that the majority of the strains investigated produced a polymer that we named cepacian,[9–13] whose chemical structure is depicted in Scheme 1. In addition to this, some strains can produce polysaccharides different from cepacian, as demonstrated by investigations carried out in a French laboratory as well as in our own,[12,14–16] The chemical structure of the repeating unit of cepacian is rather complex: it includes three saccharides in the main chain and four other saccharides in three side chains. In addition, one or two acetyl groups are present in the structure whose exact positions are not yet clarified. The repeating unit contains a rhamnose residue in the D configuration, present in the disaccharide constituting one of the side chains, and a GlcA residue in the main chain substituted on all of its hydroxyl functions. The latter characteristic certainly causes steric hindrance around the GlcA residue, affecting the overall conformational properties of the polymer chain. In fact, besides the primary structure, a knowledge of conformational characteristics constitutes basic information necessary for study of structure–function relationships. In particular, investigation of the conformational properties of cepacian is relevant in elucidating the role of specific chemical groups leading to the molecular aggregation occurring around bacterial colonies.

Previous investigations by light scattering, capillary viscometry and potentiometry showed that cepacian forms chain–chain aggregates with specific stoichiometry, and that such aggregates caused some of the carboxylic groups not to be accessible to titration.[17]

Starting from the foregoing information, this paper reports the results of conformational energy calculations and molecular dynamics (MD) simulations aimed at the defining the conformational properties of the deacetylated acidic form of cepacian both in water and in dimethyl sulfoxide (Me_2SO) a solvent often used to avoid chain–chain aggregation in solution. The elucidation of the structural features around the carboxylic group of the glucuronic acid, as well as its specific interactions with surrounding chemical groups, are described.

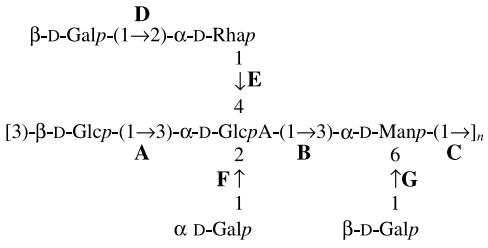

Scheme 1. Structure of the cepacian repeating unit, with indication of disaccharides connections (**A**–**G**), as referred in the text.

2. Results and discussion

2.1. Energy maps

Figure 1 shows the conformational energy maps in vacuum, calculated in the rigid residue approximation as a function of torsional angles φ and ψ for the three nearest-neighbour disaccharide units of the repeating unit of cepacian,[18,19] hereafter referred as **A**: β-D-Glc*p*-(1→3)-α-D-GlcA*p*, **B**: α-D-GlcA*p*-(1→3)-α-D-Man*p* and **C**: α-D-Man*p*-(1→3)-β-D-Glc*p*, respectively (see Scheme 1). Given the similarity of glycosidic linkage type of the three disaccharides, the overall energy surfaces of Figure 1 (b, e and c, f) showed a close resemblance to those published for the α-(1→3)-glucan disaccharides.[20] The contour diagram in Figure 1(b and e) for the **B** disaccharide had an enlarged low-energy conformational region mainly due to the angle ψ, which spans between the two gauche conformations ($-60° < \psi < 60$).

Projected onto the vacuum potential-energy maps, Figure 1 displays also 3 ns MD trajectories in water carried out on a cepacian oligomer composed of three repeating units (21 residues, Fig. 1a–c) and on the debranched cepacian (Fig. 1d–f). The dynamics of φ, ψ dihedral angles refer to the central repeating unit in the trimeric structure and define the conformation of the backbone. Despite the different force field used (as described in the experimental section), the dynamic behaviour of debranched chains (Fig. 1d–f) revealed a single localised region in the energy hyperspace practically coincident with the minima found by rigid-residue calculations. On the other hand, going to the MD results for the complete trimer structure, the data reported in Figure 1a–c showed significant differences in the accessible conformational states, which are ascribed to the influence of side chains. In all cases, the molecule explored a region of conformational space larger than that indicated by in vacuo calculations for the rigid residue.

Going to details, the trajectory showed in Figure 1a (A disaccharide) revealed a shift in the φ angle towards lower values and higher energies around the average value (φ, ψ) = (15°, −7°) ($rms_{\varphi,\psi}$ = 19, 8°), different

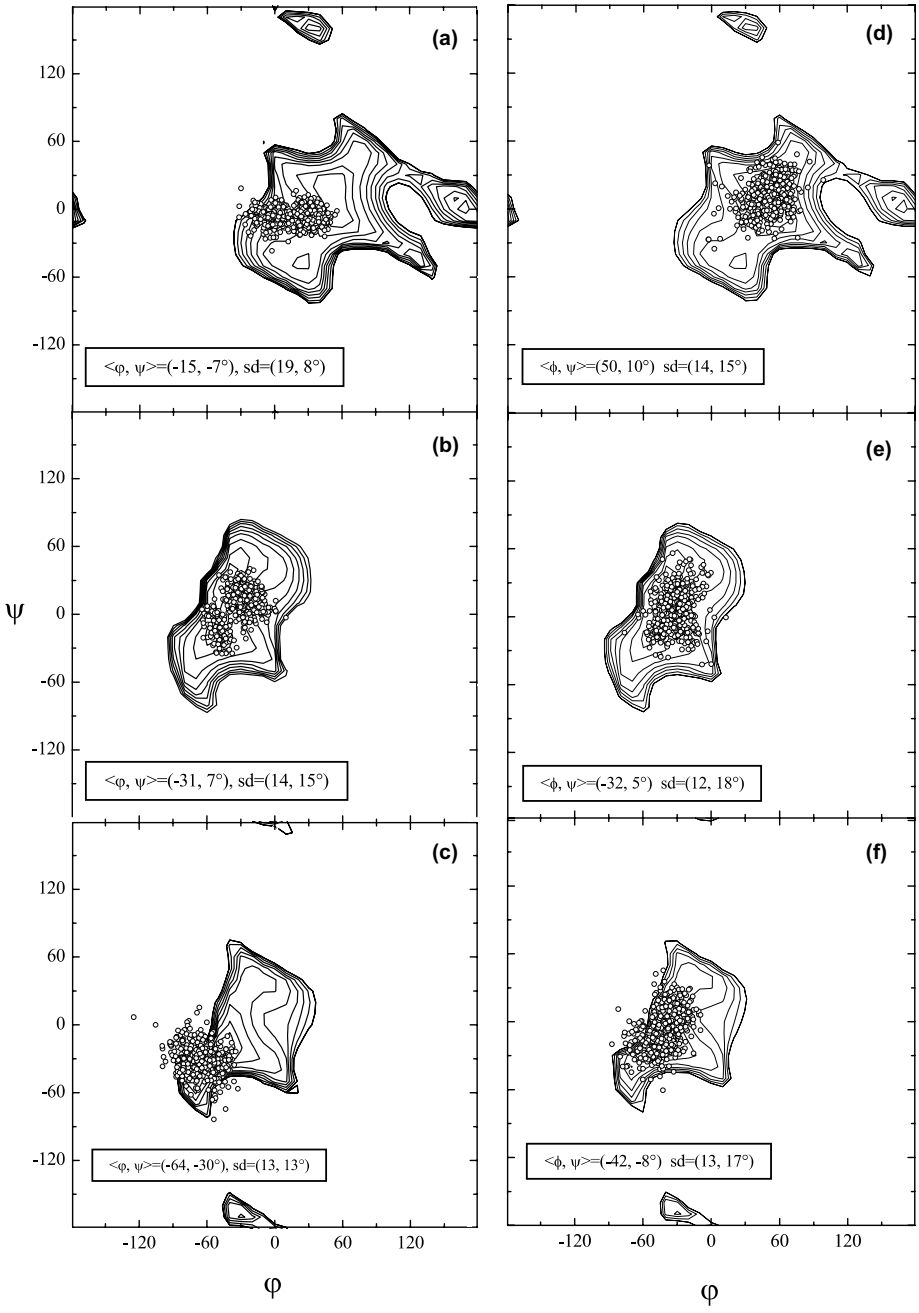

Figure 1. Rigid-residue conformational energy maps calculated for backbone representative disaccharides **A** (a, d), **B** (b, e), and **C** (c, f) in vacuum. Contours are 0.5, 1, 2,...,8 kcal mol^{-1}. Open symbols are conformational states from MD calculations of native (a, b, c) and debranched (d, e, f) polymers in water solution.

from the most stable conformation in the rigid map and attributable to side-chain interactions and the solvent effect. The same shift was not observed in the MD results for debranched chain.

The **B** disaccharide (Fig. 1b) displayed a typical example of a trajectory with a conformational transition in φ and ψ between two accessible low-energy domains crossing a barrier of few kcal mol^{-1}.

The conformational states visited by the **C** disaccharide (Fig. 1c) in the MD simulation showed a remarkable shift towards negative values, $(\varphi, \psi) = (-64°, -30°)$ with respect to the debranched case (Fig. 1f), and very close to the *gauche–gauche* conformation.

Figures 2 and 3 show the energy contours and the MD-accessible states in water of the two disaccharides forming the side chain, hereafter referred as **D**: β-D-Gal*p*-(1→2)-α-D-Rha*p* and **E**: α-D-Rha*p*-(1→4)-α-D-Glc*p*, respectively (see Scheme 1). During the 3 ns simulation, which included solvent (water) trajectories, both disaccharides were confined in a narrow region, which

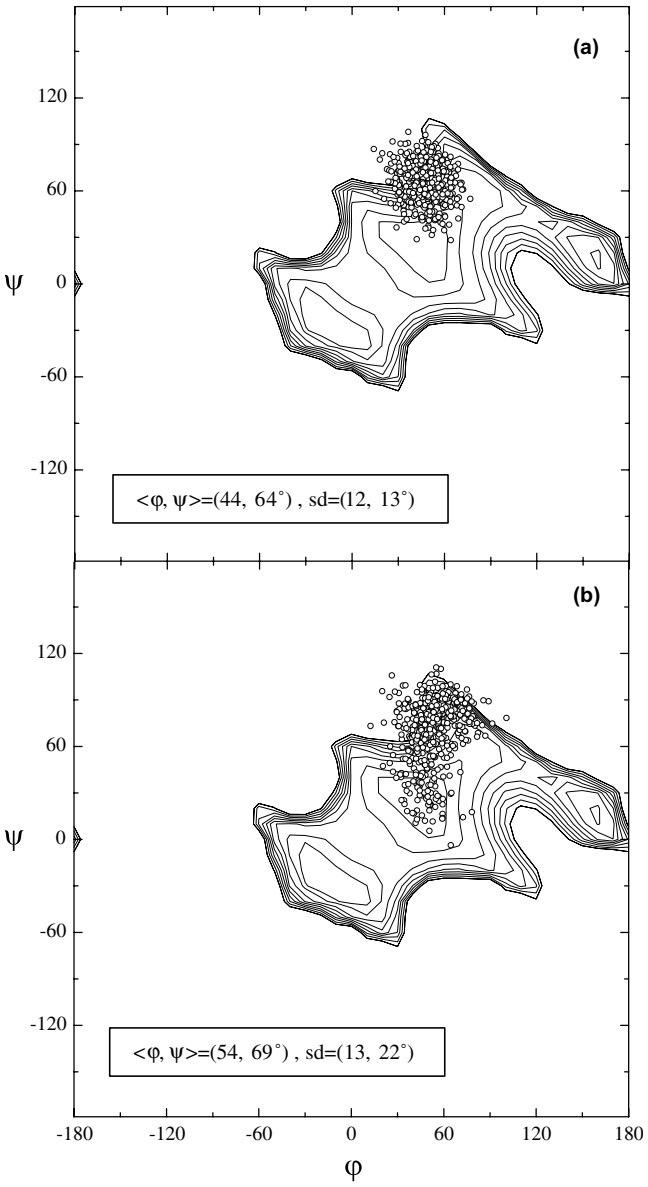

Figure 2. Conformational energy maps and MD trajectories for the **D** side-chain disaccharide in (a) water and (b) 100% Me_2SO solutions. Contours and open symbols are defined in Figure 1.

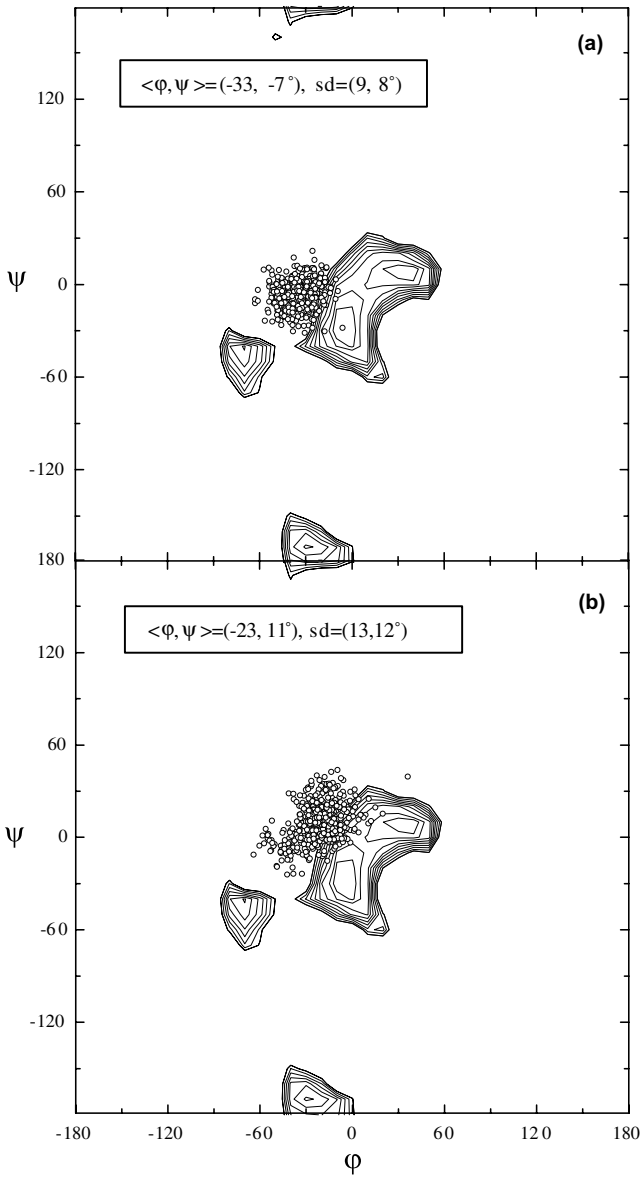

Figure 3. Conformational energy maps and MD trajectories for the **E** side-chain disaccharide in (a) water and (b) 100% Me_2SO solutions. Contours and open symbols are defined in Figure 1.

differed from that in the vacuum calculations, showing that both lateral chain–backbone and specific interactions with the solvent played an important role in the conformational wandering across the energy barrier of cepacian side chains.

Analysis of the MD data prompted a discussion on the conformational features and freedom in terms of the complexity of intramolecular hydrogen bonding (HB) occurring in the trimeric segment. The presence of solvent might affect the dynamics of the molecule in different ways, namely, by damping the overall motion of the molecule and its internal conformational fluctuations because of friction with the viscous solvent, by inducing a shift in the conformational angles, or by stimulating a transition to another conformation. In other cases, solvent molecules provided a hydrogen-bond partner to the sugar hydroxyl functions, bridging them to non-vicinal donor–acceptor groups. All of the HBs in the cepacian trimer which persisted for more than 1% of the MD total simulation time in water are shown in Figure 4 where the most significant data are those related to the inner monomer. The differences in HB percentages for the external monomers are clearly due to end effects. The most persistent hydrogen bond found in the MD simulation in water was that between the carboxyl group (donor) and 0–6 (acceptor) of the β-D-Gal residue (5 saccharide units apart) of the disaccharide (**D**) side chain (Fig. 5) belonging to the next

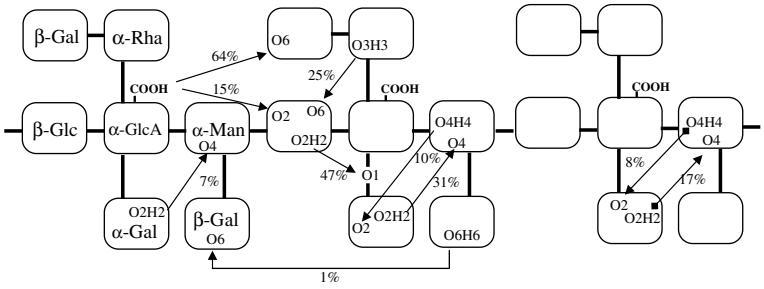

Figure 4. Schematic representation of hydrogen-bond interactions calculated for the trimer. Numeric values are the probability of HB events observed during the 3 ns simulation total time.

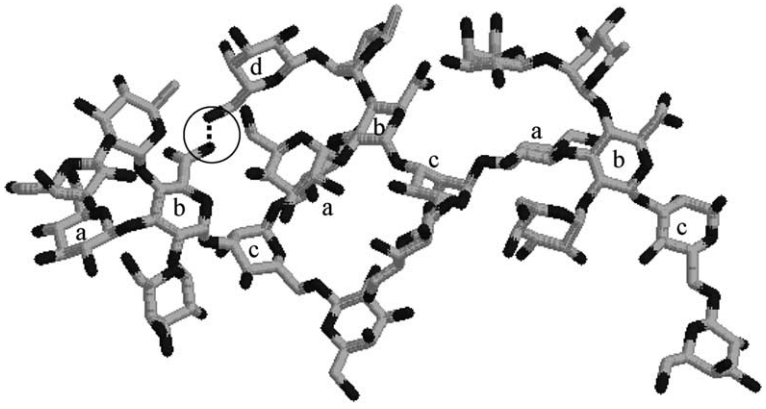

Figure 5. Snapshot of the trimer structure taken during the MD simulation in water where the molecular features of the HB between the GlcA-CO_2H (residue b) and β-Gal-6-OH (residue d) are illustrated; a, b, c indicate Glc, GlcA and Man backbone residues; d represents the β-Gal residue of the disaccharidic lateral chain.

repeating unit (64% of the total 3 ns time). In addition, the GIcA carboxyl group used 15% of the total time interacting with the O-2 acceptor of the β-D-Glc residue. Remarkably, the latter residue showed relatively strong HB interactions between its O-6 and the 3-OH group of the α-D-Rha (25% of total time) and between its 2-OH group and the anomeric O-1 of the α-D-Gal side-chain residue (47% of total time). In synergy with the interactions between α-D-Gal and α-D-Man residues (10 and 31% of the total time), the already described HBs were responsible for the very narrow dynamic fluctuations in water of the **E** and **F** (α-D-Gal*p*-(1→2)-α-D-GlcA*p* disaccharide) dihedral angles (Figs. 3 and 6, respectively). In addition, the MD trajectories for the **F** disaccharide are confined to the region of relative minimum at (φ, ψ) = (−40°, −28°) of the rigid-residue map (Fig. 6a), with no evidence for barrier crossing during the 3 ns simulation time towards the deeper minimum.

Solvent water molecules are well known to make strong hydrogen bonds with hydroxyl groups of carbohydrates, and are small enough to be inserted deep and immobilised into molecular 'cages' of given structural features. Detailed examination of MD results showed the cepacian repeating-unit conformation to be stabilised also by a water molecule that bridges the GlcA CO_2H and the β-D-Gal O-6 groups (subsequent repeating unit). Together with the experimental evidence for chain aggregation,[17] these results in water are consistent with the experimental data obtained on acid-form cepacian,[17] which indicates the carboxylic acid functionality of the exopolysaccharide to be 'screened' or otherwise suppressed in aqueous solution, with important consequences in the polyelectrolytic character and behaviour of the cepacian chain.

The (1→6)-linked β-D-Gal side chain (disaccharide **G** in Scheme 1) exhibited a weak hydrogen bond (1%) between its 6-OH group and the O-6 acceptor (see Fig. 4) of the same residue included in the preceding repeating unit. This led to a relatively high mobility of this residue, which underwent a conformational transition between the *cis* and *trans* conformers for the ϕ dihedral angle (Fig. 7a).

MD simulations in 30% Me_2SO–water mixture and pure Me_2SO (Figs. 8 and 9, respectively) showed a noticeable influence of the solvent environment on the conformational flexibility of the chain backbone. In general, the perturbation introduced by the different solvents leads principally to modification of the lower energy accessible states, and not of the overall conformational space, mainly due to the constancy of the structure-dependent repulsion-energy terms.[21] In fact, Figures 8 and 9 show that the MD populations of

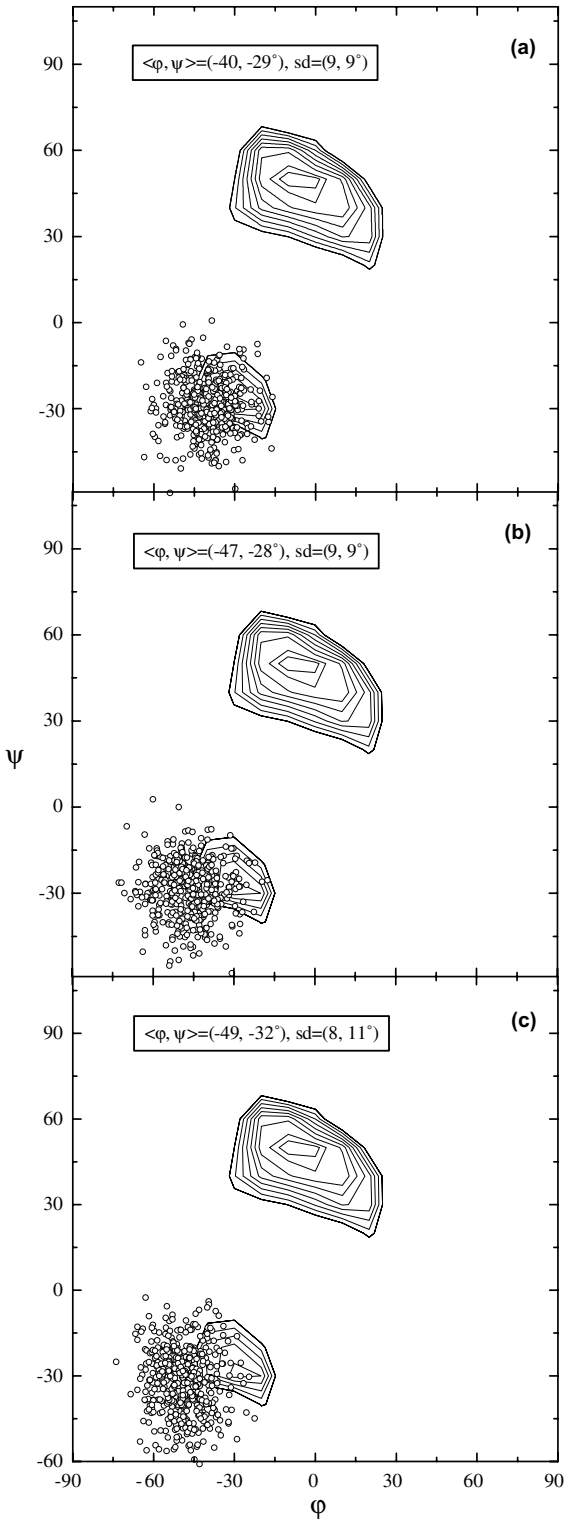

Figure 6. Conformational energy maps and MD trajectories for the **F** side-chain disaccharide calculated in (a) water, (b) 30% Me_2SO–water and (c) 100% Me_2SO solutions. Contours and open symbols are defined in Figure 1.

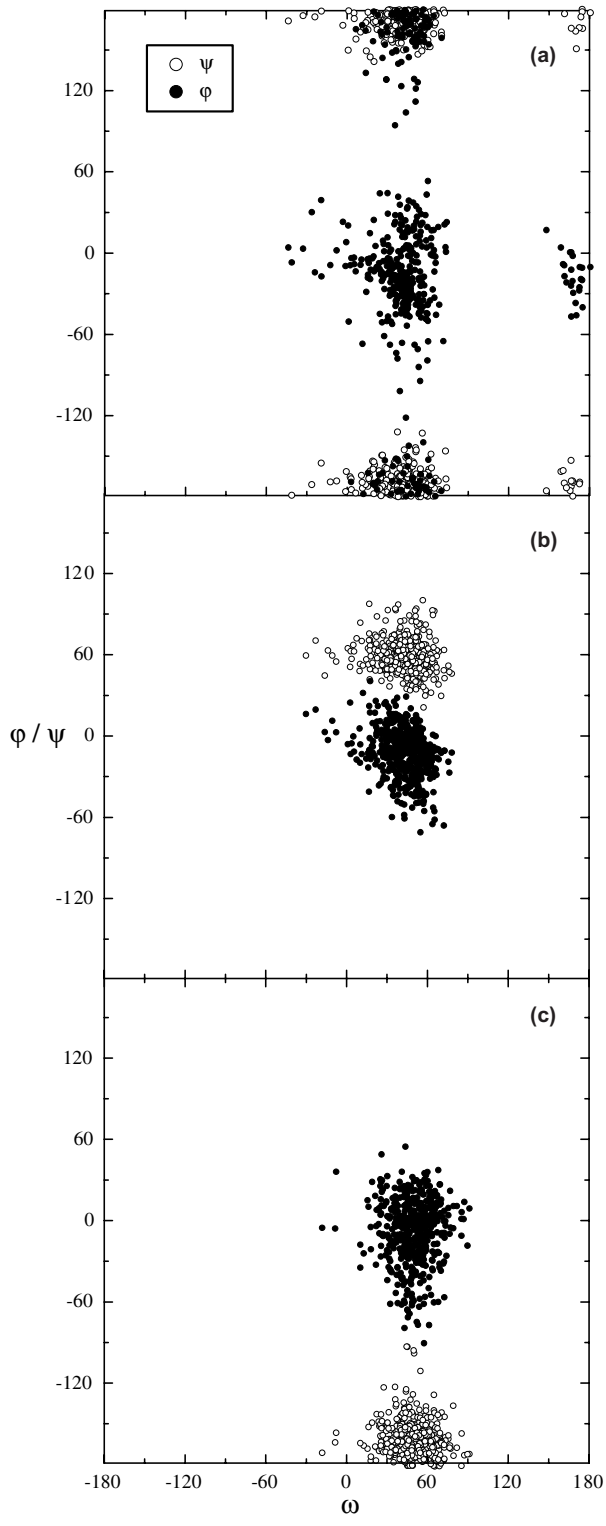

Figure 7. Conformational energy maps and MD trajectories for the **G** side-chain residue calculated in (a) water, (b) 30% Me_2SO–water and (c) 100% Me_2SO solutions. Contours and open symbols are defined in Figure 1.

accessible states did not markedly shift into conformations far from the rigid-residue low-energy region (<8 kcal mol^{-1} above absolute minima), but a relevant redistribution of favoured conformations was found with respect to the water solvent. While the **C** disaccharide unit appeared to be almost unaffected by different

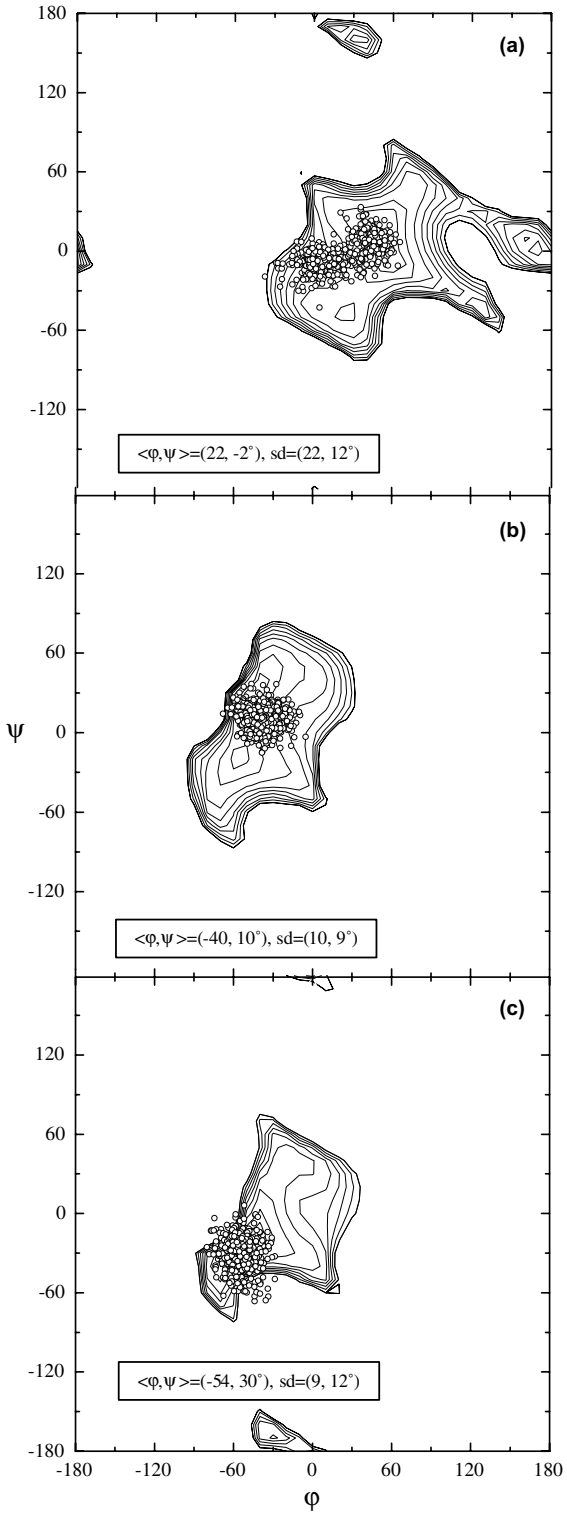

Figure 8. Rigid-residue conformational energy maps calculated for backbone representative disaccharides (a) **A**, (b) **B** and (c) **C** in 30% Me_2SO–water solution. Contours are 0.5, 1, 2,...,8 kcal mol^{-1}. Open symbols are conformational states from MD calculations.

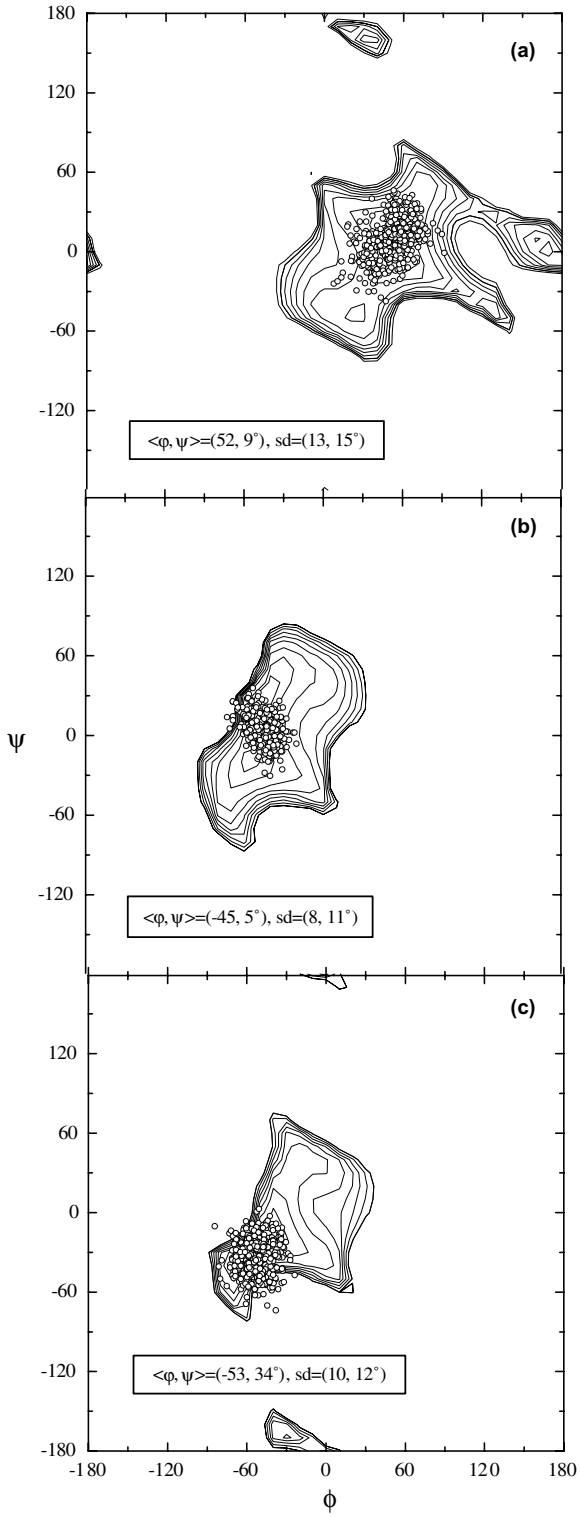

Figure 9. Rigid-residue conformational energy maps calculated for backbone representative disaccharides (a) **A**, (b) **B** and (c) **C** in Me_2SO solution. Contours are 0.5, 1, 2,...,8 kcal mol^{-1}. Open symbols are conformational states from MD calculations.

solvent conditions (Figs. 1c, 8c, and 9c), the presence of 30% Me_2SO in the MD solvent box caused for to both the **A** and **B** disaccharides significant perturbations of the preferred (φ, ψ) regions (Figs. 8a, b, 9a and b). MD energy trajectories for the β-(1→3)-linked disaccharide **A** (Figs. 8a and 9a) showed a gradual displacement

of the average conformation found in water from $\langle\varphi, \psi\rangle = (15°, -17°)$ to $\langle\varphi, \psi\rangle = (52°, -9°)$ values. These were very close to the absolute minimum of the rigid-residue map, leaving the fluctuation extent, expressed in terms of standard deviations about the mean value, almost unchanged (13–19°, 8–15° for φ and ψ, respectively). In contrast to this, solvent variations did not cause relevant conformational shifts in the average conformation of the chain fragment **B** (Figs. 1b, 8b and 9b), but the two separated populations of Fig. 1b (around $(\varphi, \psi) = (-50°, -20°)$ and $(-20°, -20°)$) disappeared and converged to a single population about $(\varphi, \psi) = (-45°, 5°)$ in the pure Me_2SO solvent, thus conferring a minor flexibility to the disaccharide unit.

Going from water to 30 and 100% Me_2SO solutions, the multiple hydrogen bonding arrangement seen in Figure 4 is strongly perturbed by Me_2SO molecules, as shown in Figure 10, where the occurrence of HB events in the 3 ns simulation time for the donor– acceptor coupling of 3-OH (α-D-Rha) and O-6 (β-D-Glc) groups are reported. After 1000 ps of equilibration time, the hydrogen-bonding events markedly decreased in 30% Me_2SO solution (Fig. 10b) and almost disappeared in pure Me_2SO (Fig. 10c). Similar behaviour was also clearly seen for the majority of the most frequent HB found for the cepacian trimer in water, as detailed in Table 1. In particular, the CO_2H donor, which is alternately or simultaneously involved in strong H bonding with the disaccharidic side chain (64% of total time) and the Glc residue in the backbone (15% of total time), became less effective in mixed and pure Me_2SO solutions, indicating the greater conformational freedom of the β-D-Gal-(1→2)-α-D-Rha side chain, as reported in Figures 2 and 3.

Considering the results for the **F** disaccharide, the data reported in Figure 6 demonstrate a strong stabilisation effect of multiple HBs involving the α-Gal residue in all solvent conditions. However, the conformationally accessible space of fragment **F** shifted by −10° in the φ dihedral angle, but was still confined in a narrow region (sd = 8°) due to the persistence of H bonding between 2-OH (β-D-Glc) and O-1 (α-D-Gal) (15%), and 2-OH (α-D-Gal) and O-4 (α-D-Man) (6%) groups, although to a lesser extent.

The β-(1→6)-linked galactose residue in the cepacian side-chain experienced only relatively weak H bonding in water (1%) between the 6-OH group and the acceptor oxygen O-6 of the same residue in the preceding repeating unit, and it appeared to be stabilised by Me_2SO molecules. In fact, the φ dihedral angle was confined around the 0° value (*cis* conformer) (Fig. 7) leaving both the ψ and ω angles unchanged to the 180° value. The forgoing discussion demonstrates the complex conformational situation of the cepacian chain, due to both its large number of monosaccharides and its peculiar branching. The conformational states described might be relevant in investigations of the interaction with other molecules.

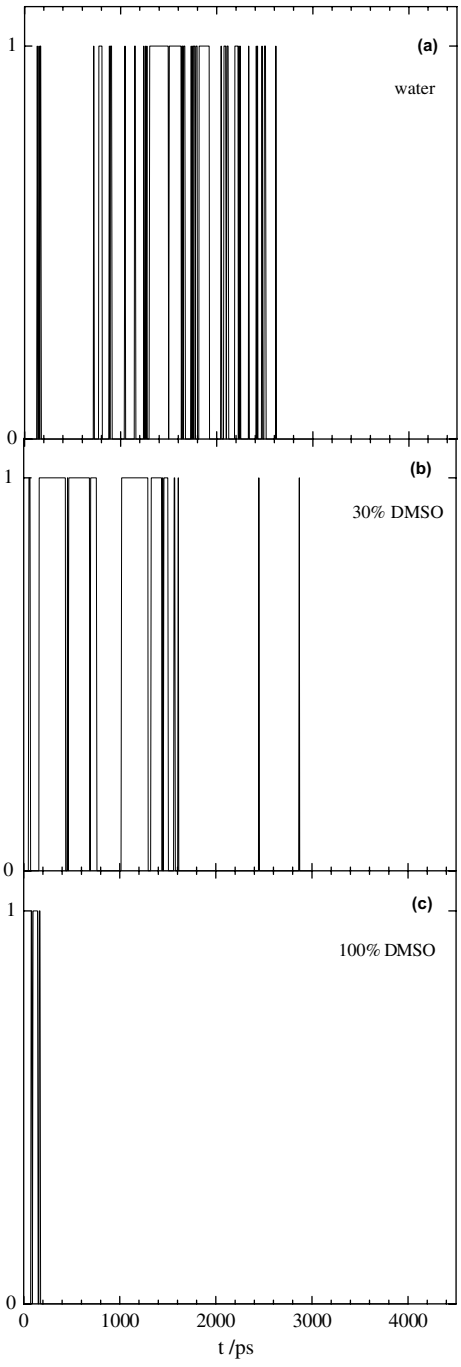

Figure 10. Occurrence of hydrogen bonding during the 3 ns simulation time for the 3-OH (α-D-Rha*p*)–O-6 (β-D-Glc*p*) interaction in (a) water, (b) 30% Me_2SO–water, and (c) 100% Me_2SO solutions.

In fact, biologically active molecules, like those activating the host immune system against bacterial infections, are considered to interact specifically with carbohydrates of bacterial complexes.

2.2. Configurational statistics

The extension and relative stiffness of the chain and the influence of solvation on the solution configuration of

Table 1. List of hydrogen bonds exhibiting the larger persistence time (% of the total dynamics simulation time) in water, 30% Me_2SO, and pure Me_2SO

H Bond donor–acceptor	Water (%)	30% Me_2SO (%)	Me_2SO (%)
CO_2H (first ru)–O-6 (β-Gal, second ru)	64	42	np
CO_2H (first ru)–O-2 (β-Glc, second ru)	15	np	np
2-OH (β-Glc, second ru)–O-1 (α-Gal, second ru)	47	33	15
3-OH (α-Rha, second ru)–O-6 (β-Glc, second ru)	25	35	2
2-OH (α-Gal, second ru)–O-4 (α-Man, second ru)	31	23	6
4-OH (α-Man, second ru)–O-2 (α-Gal, second ru)	10	3	np
6-OH (β-Gal, second ru)–O-6 (β-Gal, first ru)	0.9	0.5	np

ru = repeating unit, np = not present.

cepacian are described by the characteristic ratio (C_x), the persistence length (L_x) and the virtual-bond correlation function (F_x). These parameters were evaluated from the statistical Monte Carlo (MC) samples as a function of x, the number of monomeric or monosaccharidic units, by using a home-made software program.[22] The MD populations reported in Figures 1, 8 and 9 were used as the basis for evaluating the probabilities associated with accessible conformational states. Computed values of C_n and L_n are presented in Figure 11 as a function of $n = 3N$, where N is the number of backbone repeating units and n is the number of the backbone monosaccharide residues. The C_n curves in the three solvents reached monotonically the asymptotic value, C_∞, at different degrees of polymerisation, n, with different rate of convergence to C_∞. The rate of convergence is usually expressed by the value $N(95\%)$ defined as the length necessary for the chain to achieve 95% of the Gaussian condition. The calculated results (Table 2) showed for C_∞ of cepacian polymer, in water and 30% Me_2SO solutions values of 14 and 24, respectively, which are of the same order as that found for a (1→3)-D-glucan (pseudonigeran) by Brant and Burton[19] in vacuo ($C_\infty = 32$). The $N(95\%)$ values in these conditions were very high because after only 139 and 169 monomeric units, the chain reached the Gaussian behaviour in water and 30% Me_2SO, respectively. In addition, a high directional persistence of the chain was observed, in agreement with the persistence length parameter L_∞ (Table 2). The shape of the bond-correlation function F_n as a function of n, which is the mean projection of a unit vector along the nth virtual bond describing the chain (distance between glycosidic oxygens) onto a unit vector aligned with the first virtual bond, is very interesting. Figure 12a and b (water and 30% Me_2SO, respectively) shows a rapid decay of F_n after the first seven residues, followed by a negative part for $n = 8$–15, as the consequence of the mean opposite direction of these residue vectors with respect to the first one. This oscillating character up to 60 residues reflected a pseudo-helical order of the backbone trajectory of relatively long segments of the chain containing approximately 22 monosaccharide units in each period. Superimposed on the low-frequency periodic character, there were also lower periodic oscillations of 2–3 residues (Fig. 12), which were not strongly correlated to the shapes of the conformational energy surfaces, but rather with the nature of the backbone glycosidic linkages. Differences in the linkage topology, expressed in terms of dihedral and bond

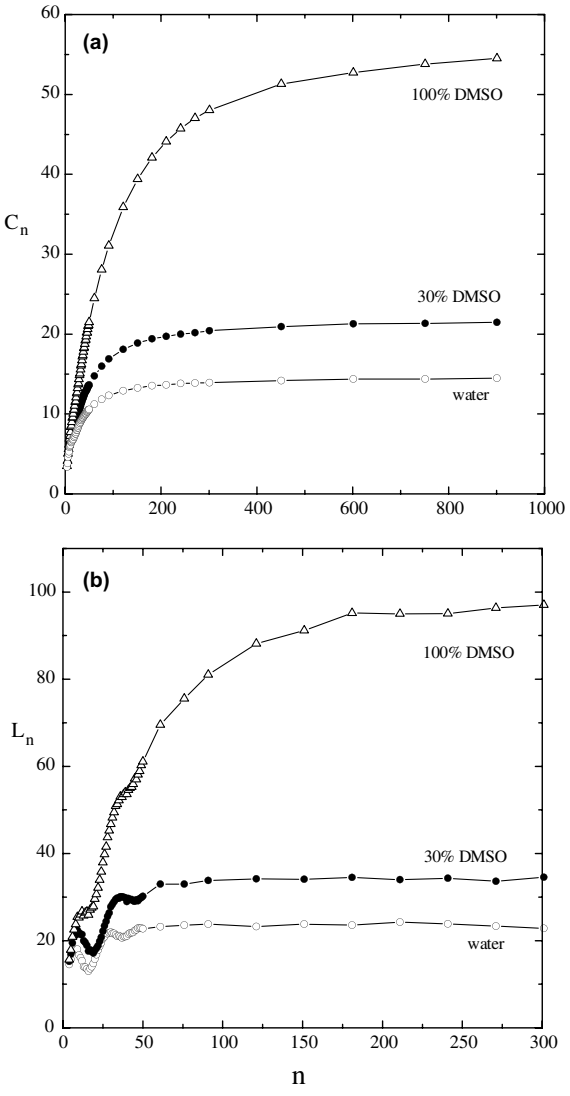

Figure 11. Characteristic ratio C_n (a) and persistence length L_n (b) as a function of the backbone monosaccharide units n in water, 30% Me_2SO–water and 100% Me_2SO solutions.

Table 2. Characteristic ratio, persistence length and rate of convergence to C_∞ of the cepacian chain in different solvent conditions

	Water	30% Me_2SO	100% Me_2SO
C_∞	14	21	58
L_∞	24	35	97
N(95%)	139	169	870

angles of virtual bonds, introduced an abrupt change in the direction of chain propagation at residues for $n = 6$, 9, 12, 15, 18,... up to $n = 30$ (Fig. 12). The foregoing residue numbers corresponded to the mannose monosaccharide units. In fact, the virtual dihedral and bond angles of mannose suggested a disruption of the relatively rectilinear propagation of the preceding disaccharide β-D-Glc-(1→3)-α-D-GlcA along the chain.

Changing the solvent condition to pure Me_2SO had a dramatic effect on the characteristic ratio of cepacian chain, with C_∞, and L_∞ values predicted to increase by 2-fold (58) and 3-fold (97), respectively. This was in good agreement with data reported for many polysaccharides,[23–25] showing that the specific solvation in Me_2SO solution gave rise to considerably larger values of radii of gyration and second virial coefficients than in water solution. Longer decays of correlation functions and a shift towards less negative values were found in 30% water–Me_2SO and in pure Me_2SO (Fig. 12b and c, respectively), reflecting the tendency to achieve more-extended conformations in solution. In addition, the chain dimensions and features of cepacian in Me_2SO resemble those of debranched chains (data not reported), which exhibit $C_\infty = 42$ and $L_\infty = 86$, together with poor helicoidal character, indicating a highly extended chain with great directional persistence (N(95%) = 124).

In conclusion, the molecular modelling calculations carried out on the cepacian chain indicated that polymer conformational features are affected by the lateral chains, but are also largely dictated by the presence of solvent. In fact, the extended hydrogen bonding in water disappeared in Me_2SO solution, giving rise to an extended chain similar to that obtained for the debranched polymer. The HB system also involves a water molecule immobilised onto the carbohydrate polymer. In addition, these interactions lead the carboxylate group of the GlcA residue to interact strongly with neighbour residues of both the main chain and the disaccharideic lateral chain, rendering it poorly approachable by solvent and other small molecules. The chain possesses a pseudo-order at short as well as at long range, producing both elongated and bent sequences, the latter with a large bending radius. The tendency of the cepacian backbone to form these structures is shown in Figure 13, where two-chain snapshots obtained by MC calculation are reported.

The above-described conformational and structural features are in very good agreement with the macro-

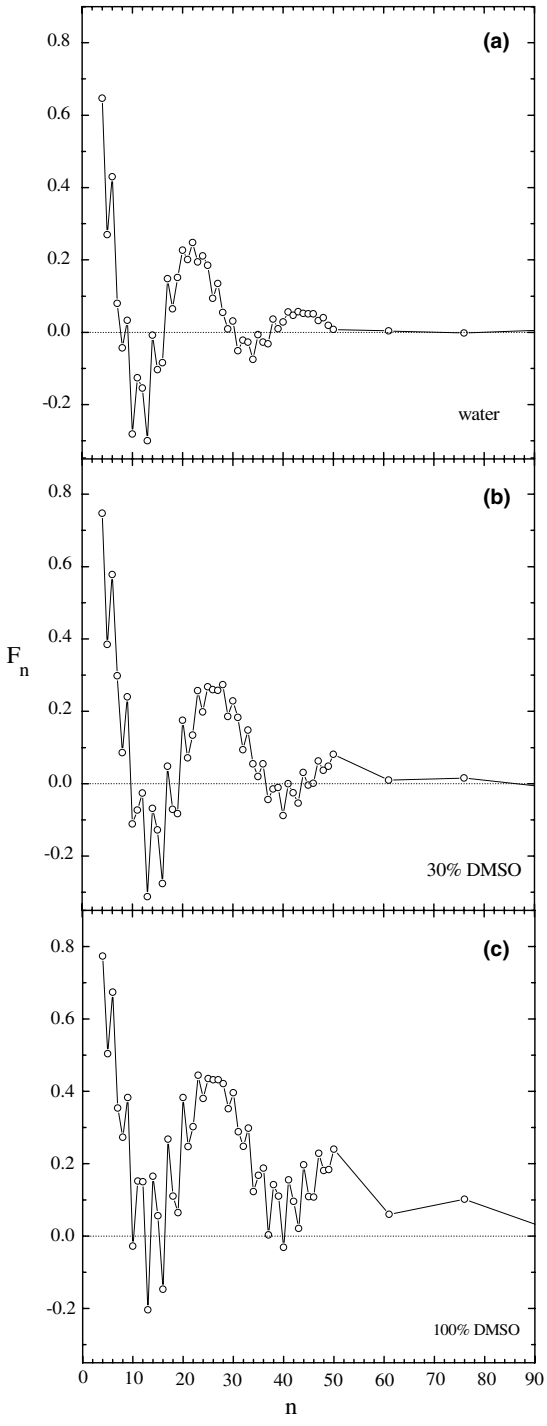

Figure 12. Dependence of the correlation function F_n on the number of the backbone monosaccharide units n calculated in (a) water, (b) 30% Me_2SO–water and (c) 100% Me_2SO solutions.

molecular characteristic defined by light scattering as well as capillary viscometry experiments.[17] In addition, the rather high chain rigidity, which implies a large excluded volume, might explain the ability of the polymer to form extended networks around bacterial colonies, helping them to survive in such stress conditions as those present in fibrotic lungs.

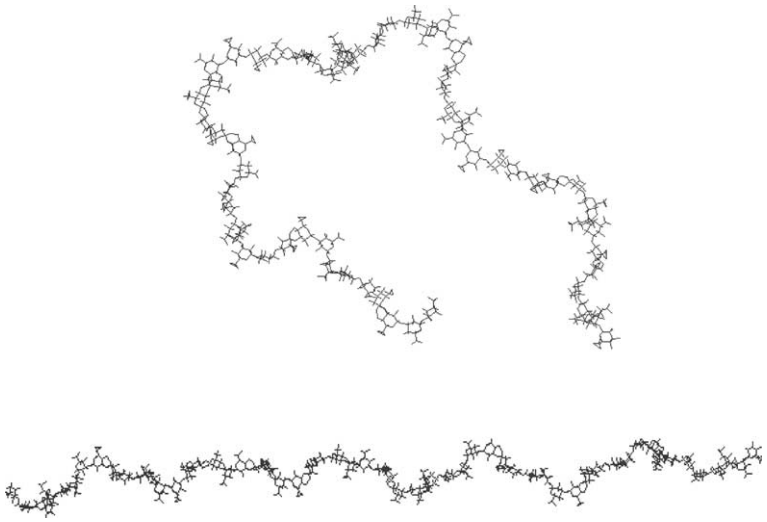

Figure 13. Snapshots of two cepacian chain segments showing different end-to-end distances as obtained from MC calculations in water.

3. Experimental

3.1. Energy and molecular dynamics calculations

In this paper two methods were used to study the conformational features of cepacian chains: the molecular-dynamics simulation of the trimer of cepacian polysaccharide in different solvents and the Monte Carlo (MC) method for the statistical features of cepacian polymer. Moreover, Ramachandran energy maps were also computed, using the Brant force fields and charges[35] in the rigid residue approximation and taking into account only the nearest-neighbour interactions between adjacent monosaccharides in the chain. Although these approximations are often removed in current MM simulations, the comparison between MD and the rigid residue conformational states was made, considering that the overall accessible conformational space is mainly dependent on the repulsive term in the potential energy function.

In the MD computations a modified version (parameters and partial charges) of the GROMOS 96 force field[26] for carbohydrates as proposed by Pereira et al. (Ref. 27 and personal communication) has been used. The set 45A3 of the Gromos force field were changed, mainly by a new set of partial charges and some appropriate dihedral parameters for the hydroxymethyl groups (Lins P.H. and Hunenberger P.H., unpublished results). Anomeric and exoanomeric effects were also taken into account. Saccharide units maintained the $^4C_1$ conformation during MD tests, although some short-time fluctuations (lower than 5 ps) were observed for single residues. Molecular dynamics simulations longer 3 ns for the disaccharides present in cepacian were run, and the conformational space visited agreed quite well with the conformational states obtained using the MM3 force field in the SWEET home page.[28]

The geometry of the cepacian trimeric oligomer was obtained from the SWEET home page.[28] This molecule was optimised by 10,000 steps of conjugate gradient and a cycle of steepest descent was performed every 1000 steps. Although no systematic search for the global minimum energy was performed, several starting conformations were tested using the foregoing minimization protocol. A quenching dynamics at a initial temperature of 700 K was also performed. The final conformation obtained was determined to be energetically the more stable one, and any other conformation was at least 20 kcal mol^{-1} higher. The molecule then was introduced in a previously thermalised solvent box. Water, dimethyl sulfoxide (Me_2SO) and Me_2SO–water mixtures (~30 % v/v) were used as solvents. Solvent molecules that approached the cepacian atoms closer than the sum of their van der Waals radii were excluded. The dimensions of boxes, number of solvent molecules, as well as other parameters used in the dynamical runs are listed in Table 3. The simulations were performed in the NpT ensemble at 300 K and 1 atm. Both temperature and pressure were modulated using the weak coupling technique[29] with coupling constant and isothermal compressibility parameters shown in Table 3. Periodic boundary conditions were imposed and all bonds were constrained using LINCS[30] and SHAKE[31] algorithms, leading to a time step of 2 fs for integrations of the equations of motion. The electrostatic interactions were corrected using the reaction field[32] approximation with proper dielectric constants. For thermalisation, the minimised trimers time were maintained fixed for a 500 ps simulation to relax the solvent box and the MD total time were of 3 ns. In order to test the validity of the 3 ns simulation time, some calculations were performed for 6 ns without significant changes in conformer populations. All data analysis was made using the facilities of the GROMACS package.

Table 3. Parameters and conditions used in conformational energy calculation and molecular dynamics simulation

Conditions	
Energy minimisation	5000 cg steps
Position restrain	100 ps
Thermalisation time	1 ns
Total time	3 ns
Box size	$6 \times 6 \times 6$ nm^3 except for 100% Me_2SO ($5.88 \times 5.88 \times 5.88$)
Timestep	0.002 ps
Non-bonded correction	Reaction field
Temperature coupling	Berendsen[14–16]
Coupling time constant	0.05 ps (solvent), 0.5 (sugar)
Bath temperature	300 K
Pressure coupling	Berendsen[14–16]
P Coupling constant	0.5 ps, 1.0 (100% Me_2SO run)
Reference pressure	1 atm

The dihedral torsion angles were obtained from the intermediate residue in the trimer in order to simulate the continuity existing in the chain and adding or subtracting the proper difference (~120°) to the crystallographic dihedral angles. Thus, in this paper the pairs (φ, ψ) refer to the **H** atom bonded to the respective carbon atom for each linkage and in according to the rules recommended by the IUPAC-IUB convention.[33] The torsional angles are therefore defined as

$$\varphi = \text{H-1–C-1–O-1–C}_m$$

$$\psi = \text{C-1–O-1–C}_m\text{–H}_m$$

$$\omega = \text{O-1–C-6–C-5–H-5}$$

where *m* is the atom involved in the glycosidic linkage.

3.2. Statistical methods

The cepacian chains were built using the Monte Carlo method as proposed by Brant and co-workers,[34] based on surface probability maps by using a virtual bond connecting the glycosidic bond oxygen atoms of the backbone. Three different probability maps were considered, namely: β-D-Glcp-(1→3)-α-D-GlcA*p*, α-D-GlcA*p*-(1→3)-α-D-Man*p* and α-D-Man*p*-(1→3)-β-D-Glc*p*, obtained from the MD trajectories for each set of solvent conditions considered in the computation. A probability distribution function was computed over all conformational states (500–600) accessible to the trimer in the 3 ns simulation time. Average properties were computed on MC samples of 100,000 up to 1,000,000 chains as a function of backbone monosaccharide unit, *n*, or of backbone monomeric unit, *N*. The convergence was also tested as a function of number of chains of the MC sample. A standard deviation less than 0.1% on the characteristic ratio and persistence length was obtained for samples composed by 100,000 or more chains.

Macromolecular features of the cepacian chain were evaluated by mean of the characteristic ratio, C_n, persistence length, L_n and correlation function, F_n, as defined elsewhere.[22]

Acknowledgements

The Regione Friuli-Venezia Giulia Regional Government (Italy) and Fondazione Cassa di Risparmio (Trieste, Italy) are acknowledged for financial support. CAPES (Brazil) is acknowledged for the fellowship to C.E.S.N.

References

1. Burkholder, W. H. *Phytopathology* **1950**, *40*, 115–117.
2. Govan, J. R. W.; Deretic, V. *Microbiol. Rev.* **1996**, *60*, 539–574.
3. Govan, J. R. W.; Hughes, I. E.; Vandamme, P. *J. Med. Microbiol.* **1996**, *45*, 395–407.
4. Mahenthiralingam, E.; Baldwin, A.; Vandamme, P. *J. Med. Microbiol.* **2002**, *51*, 533–538.
5. May, T. B.; Shinabarger, D.; Maharaj, R.; Kato, J.; Chu, L.; de Vault, J. D.; Roychoudhury, S.; Zielinski, N. A.; Berry, A.; Rothmel, R. K.; Misra, T. K.; Chakrabarty, A. M. *Clin. Microbiol. Rev.* **1991**, *4*, 191–206.
6. Chung, J. W.; Altman, E.; Beveridge, T. J.; Speert, D. P. *Infect. Immun.* **2003**, *71*, 904–909.
7. Hostetter, M. K.; Thomas, M. L.; Rosen, F. S.; Tack, B. F. *Nature* **1982**, *298*, 72–75.
8. Pier, G. B.; Coleman, F.; Grout, M.; Franklin, M.; Ohman, D. E. *Infect. Immun.* **2001**, *69*, 1895–1901.
9. Cerantola, S.; Lemassu-Jacquier, A.; Montrozier, H. *Eur. J. Biochem.* **1999**, *260*, 373–383.
10. Cescutti, P.; Bosco, M.; Picotti, F.; Impallomeni, G.; Leitão, J. H.; Richau, J.; Sá-Correia, I. *Biochem. Biophys. Res. Comm.* **2000**, *273*, 1088–1094.
11. Linker, A.; Evans, L. R.; Impallomeni, G. *Carbohydr. Res.* **2001**, *335*, 45–54.
12. Lagatolla, C.; Skerlavaj, S.; Dolzani, L.; Tonin, E. A.; Monti Bragadin, C.; Bosco, M.; Rizzo, R.; Giglio, L.; Cescutti, P. *FEMS Microbiol. Lett.* **2002**, *209*, 89–94.
13. Chiarini, L.; Cescutti, P.; Drigo, L.; Impallomeni, G.; Herasimenka, Y.; Bevivino, A.; Dalmastri, C.; Tabacchioni, S.; Manno, G.; Zanetti, F.; Rizzo, R. *J. Cyst. Fibrosis* **2004**, *3*, 165–172.
14. Cerantola, S.; Marty, N.; Montrozier, H. *Carbohydr. Res.* **1996**, *285*, 59–67.
15. Cerantola, S.; Montrozier, H. *FEMS Microbiol. Lett.* **2001**, *202*, 129–133.
16. Cescutti, P.; Impallomeni, G.; Garozzo, D.; Sturiale, L.; Herasimenka, Y.; Lagatolla, C.; Rizzo, R. *Carbohydr. Res.* **2003**, *338*, 2687–2695.
17. Sist, P.; Cescutti, P.; Skerlavaj, S.; Urbani, R.; Leitão, J. H.; Sá-Correia, I.; Rizzo, R. *Carbohydr. Res.* **2003**, *338*, 1861–1867.
18. Urbani, R.; Di Blas, A.; Cesàro, A. *Int. J. Biol. Macromol.* **1993**, *15*, 24–29.

19. Brant, D. A.; Christ, M. D. In *Computer Modeling of Carbohydrate Molecules*; French, A. D., Brady, J. W., Eds.; ACS Symposium Series; Washington, DC; 1990; No. 430, Chapter 4.
20. Burton, B. A.; Brant, D. A. *Biopolymers* **1983**, *22*, 1769–1792.
21. Urbani, R.; Cesàro, A. *Polymer* **1991**, *32*, 3013–3020.
22. Ruggiero, J. R.; Urbani, R.; Cesàro, A. *Int. J. Biol. Macromol.* **1995**, *17*, 213–218.
23. Jordan, R. C.; Brant, D. A. *Macromolecules* **1980**, *13*, 491–499.
24. Burchard, W. *Makromol. Chem.* **1963**, *64*, 110–121.
25. Straub, P. R.; Brant, D. A. *Biopolymers* **1980**, *19*, 639–643.
26. van Gunsteren, W. F.; Berendsen, H. J. C.; Gromos-87 Manual. Biomos BV Nijenborgh 4, 9747 AG Groningen, The Netherlands, 1987.
27. Pereira, C. S.; Lins, R. D.; Chandrasekhar, I.; Freitas, L. C. G.; Hunenberger, P. H. *Biophys. J.* **2004**, *86*, 2273–2285.
28. Bohne, A.; Lang, E.; von der Lieth, C. W. *Bioinformatics* **1999**, *15*, 767–768.
29. Berendsen, H. J. C.; Postma, J. P. M.; Van Gunsteren, W. F.; Di Nola, A.; Haak, J. R. *J. Chem. Phys.* **1984**, *81*, 3684–3690.
30. Hess, B.; Bekker, H.; Berendsen, H. J. C.; Fraaije, J. G. E. M. *J. Comp. Chem.* **1997**, *18*, 1463–1472.
31. Ryckaert, J. P.; Ciccotti, G.; Berendsen, H. J. C. *J. Comp. Phys.* **1977**, *23*, 327–341.
32. Tironi, I. G.; Spub, R.; Smith, P. E.; van Gunsteren, W. F. *J. Chem. Phys.* **1995**, *102*, 5451–5459.
33. IUPAC—IUB Commission for Biochemical Nomenclature. *Arch. Biochem. Biophys*., **1971**, *145*, 405–421.
34. Jordan, R. C.; Brant, D. A.; Cesàro, A. *Biopolymers* **1978**, *17*, 2617–2632.
35. Goebel, C. V.; Dimpfl, W. L.; Brant, D. A. *Macromolecules* **1970**, *3*, 644–654.